Validation of heartrate data, measured during a resting state fMRI-scan

B. Meuter

Supervisors: A. Brehl, N. Kohn, G. Fernández

Donders Institute for Brain, Cognition and Behavior, Centre for Neuroscience, P.O. Box 9010, 6500 GL Nijmegen, The Netherlands

Article info:

Keywords:
Heart rate, validation
heart rate variability,
central autonomic network,
autonomic nervous system,
anxiety

Date:
9 Juli 2021

Abstract

The central autonomic network (CAN), including brain regions that are affected in anxiety disorders, is involved in the autonomic nervous system (ANS) of the body. The ANS modulates the heart via the vagus nerve that projects on the sinoatrial node. Measures of heart rate variability (HRV) are often used as indicator of this influence. However, the reciprocal effect of the heart on brain regions is often considered an undesired signal.

In order to validate cardiac data for studying HRV in an anxious population, we correlated instantaneous heart rate (HR) with voxel-wise fMRI-data from a highly anxious population including 190 participants.

We found large correlations between the instantaneous HR and pulsating fluids in the brain (arterial/venous blood and CSF) which is evidence that the data is valid. Additionally, we found associations between HR and regions associated with the CAN including the medial prefrontal cortex, anterior cingulate cortex, precuneus, and cerebellum.

Taken together, the cardiac data from the large anxious population is valid and allows investigation of the autonomic relation between the heart and the brain via HRV.

1. Introduction

The role of the heart in modulating neural cognitive functions and activity has been suggested more than 50 years ago (Lacey, 1967). Since this suggestion, many researchers in the field of neurocardiology, which aims to find functional and anatomical connections between the heart and the brain, studied how the response from the heart affects specific brain functions, and later how the brain modulates the heart dynamics (Shaffer et al., 2014). Several feedback and control mechanisms in the body regulate the HR. The sinoatrial (SA) node and atrioventricular (AV) node are pacemakers of the heart and spontaneously generate potentials without the need of external stimulation. In a healthy heart, the SA node is the primary initiator of a heart contraction. The autonomic nervous system (ANS) plays a key role in adjusting the intrinsic firing rate of the SA node (60-100 action potentials per minute) (Shaffer et al., 2014). Many processes and sensors in the body influence the ANS. A correct working ANS is important for neural health, dysregulation of the ANS is a common finding in a variety of psychiatric disorders including depression, and anxiety (Kamath et al., 2013).

The ANS is subdivided in an excitatory sympathetic nervous system (SNS), which is counterbalanced by the inhibitory parasympathetic nervous system (PNS). One of the effects of the SNS is heart rate (HR) acceleration and the PNS slows HR. The ANS is modulated by information from proprioceptors (body position), baroreceptors (blood pressure), chemoreceptors (blood chemistry) from the heart, and neural information from cerebral cortex and limbic system that are integrated in the medulla of the brainstem. These systems alter the balance between the SNS and PNS, resulting in an excitatory or inhibitory net autonomic outflow to the heart, resulting HR to increase or decrease. The rate of change in HR frequencies is called the heart rate variability (HRV). At rest, the PNS predominates, resulting in an HR of ±75 beats per minute (bpm) (Shaffer et al., 2014). Brain regions involved in autonomic control of the heart have been referred to as the central autonomic network (CAN), consisting of a network of forebrain and brainstem components (Benarroch, 2012; Valenza et al., 2019). Classically, forebrain components including the insular cortex, amygdala, medial prefrontal cortex (mPFC) and several regions of the hypothalamus integrate pain and bodily sensation (bottom-up inputs) with goal-related and emotional autonomic top-down responses (Benarroch, 2012, 1993). Additionally, studies using functional magnetic resonance imaging (fMRI), which measures the blood oxygen level dependent (BOLD) response of the brain, identified more structures involved in the CAN such as the anterior cingulate cortex (ACC), thalamus, hippocampus (HC), precuneus (PC), and cerebellum which also have been involved in important ANS functions (Sklerov et al., 2019). Immediate and reflective control of circulation, respiration, gastrointestinal, and micturition are controlled by brainstem areas including the parabrachial nucleus (PBN), the periaqueductal gray of the midbrain (PAG), and areas in the medulla (Benarroch, 2012).

Several studies explored the relation between the heart and brain including a variety of tasks that influence the autonomic SNS-PNS balance. Many of them focused on the high frequency (HF) content of HRV, which is found to be an indicator for parasympathetic activity, where the low frequency (LF) content indicates mixed PNS and SNS activity (Critchley et al., 2003; Kim and Yoon, 2018; Lane et al., 2009; Napadow et al., 2008; Valenza et al., 2019). Only few studies included and reported correlations between HR and neural activity measured using fMRI during resting-state (RS) condition (Nikolaou et al., 2016; Valenza et al., 2019). Differences in BOLD responses to find task-induced brain activity is often used in fMRI studies. However, some are interested in the neural correlates in a task-free RS condition. Nikolaou et al. (2016) were interested in the influence of physiological fluctuations on BOLD signal and revealed an effect of time varying properties of HR/HRV in neural activity within the somatosensory and visual resting-state networks. Valenza et al. (2019) investigated correlations between voxel-wise fMRI data and continuous HR-data in rest. They found positive significant correlations in brain regions including the left frontopolar cortex (FPC), left dorsomedial PFC (dmPFC), right superior frontal gyrus (SFG), a regions in the anterior, middle and posterior cingulate cortices (ACC/MCC/PCC), left superior parietal lobule, PC, right angular gyrus, cerebellar regions and right primary visual cortex (Benarroch, 1993; Valenza et al., 2019).

HRV is commonly used in research as indicator for psychological wellbeing and is found to be reduced in association with higher levels of worry, hypervigilance, and a variety of anxiety disorders (Chalmers et al., 2014). According to the neurovisceral integration model, efferent nerve fibers from the PFC modulate parasympathetic activity and vagal nerve inhibition of cardiac activity, which are important regulators in the ability to adaptively respond to environmental, physiological, cognitive, behavioral and emotional influences (Chalmers et al., 2014). The CAN is a key feature in this model, from which the integrity is compromised in anxiety; excitatory SNS responses are unable to be effectively inhibited by the PNS (Chalmers et al., 2014). Parasympathetic vagal nerve activity controls the heart by modulating and projecting on the the SA-node (Sološenko et al., 2015). Therefore, it is important to focus on heart contractions that are stimulated by the SA-node. However, ectopic beats such as premature ventricular contractions (PVCs) are initiated by secondary pacemakers (ectopic foci) that are located in the ventricles of the heart (Kamath et al., 2013; Shaffer and Ginsberg, 2017; Sološenko et al., 2015). These beats should be detected and removed. Measures of HRV during cognitive and emotional tasks could be an indicator of impaired prefrontal control in a highly anxious population (Thayer et al., 2012). However, in order to investigate HRV and study the relationship with neural activity, the peripherally measured HR-data has to be validated whether it can be used for brain correlations. If the data is validated, we will investigate what brain areas are active in controlling the HR or are affected by the HR.

The aim of this study is to test for validation of HR-data, obtained with a pulse oximeter during a resting state (RS) fMRI scan, by correlating the HR with voxel-wise analyses of simultaneously measured fMRI data. The data is obtained from a large study, including highly anxious participants, focusing on the neural correlates of anxiety (Brehl et al., 2021). Additionally, we would like to obtain a better understanding of brain regions that are involved in RS heart rate modulations in the highly anxious population. Furthermore, the results will be compared to findings of earlier studies that investigated the relation between heartrate and neuronal data during RS. The HR-data will be validated by finding correlations with several brain regions involved in the CAN, and showing similar results compared to previous studies. However, based on previous analysis using the HR-data from this experiment, we have reasons to believe the data is invalid. The study included a threat of shock task, where the participant were presented a red or green border on the screen. While the red border was shown, the participants could receive a shock, and when a green border was shown they were safe. According to literature, HR during threat conditions compared to safe would be higher (Smith et al., 1985). In contrast, our HR-data showed the opposite effect for periods of threat compared to safe. Therefore, we believe that validation of the HR-data will fail.

2. Methods

2.1 Participants

The study included 246 subjects collected from a larger study (178 females, 68 males) aged between 18 and 48 (mean = 23.0; SD = 5.3) (Brehl et al., 2021). The subjects were selected from a large cohort who filled in the hospital anxiety and depression scale – anxiety subscale (HADS-A) questionnaire. To account for oversampling, those who showed high (>7) HADS-A scores had 100% chance of being invited for the study, subjects who had HADS-A scores equal or below 7 had 25% chance of being included in the study. In the current study, participants were excluded if they used drugs in the week before the experiment, fell asleep during the experiment, had incomplete data, and when they had bad data quality for at least one of the measures, fMRI or HR, as specified in the following paragraphs.

2.2 RS-run

The large study consisted of four different tasks that were performed in an fMRI-scanner; Hariri, threat of shock, emotion regulation, and at the end RS (±420s) (Brehl et al., 2021). During the RS-task, subjects were instructed to look at a cross that showed on the screen in the scanner while being scanned and measured with a pulse oximeter applied at the finger.

2.3 fMRI data acquisition

Whole-brain imaging data was obtained using a 3T Magnetom PrismaFit MRI scanner (SiemensAG, Healthcare Sector, Erlangen, Germany) with a 32-channel head coil. For each participant, fMRI data was obtained using echo-planar imaging (EPI)-based multiband 4 sequences with the following settings: slice number = 68, repetition time (TR) = 1500ms, echo time (TE) = 39.6ms, flip angle = 75 deg, voxel size = 2x2x2 mm, slice skip = 0mm and the field of view (FOV) was 210x210x210 mm. The RS-scan consisted of ±280 whole brain volume images that were obtained during 420 seconds (280 x TR). For anatomical reference a high-resolution T1-weighted image was obtained with the following settings: 192 slices with TR = 2300 ms, TE = 3.03ms, flip angle = 8 deg, voxel size = 1x1x1 mm, FOV = 256x256x192 mm, base resolution = 256 mm, sagittal acquisition orientation.

2.4 HR-data acquisition

Photoplethmysography (PPG) waveforms were acquired using the pulse oximeter (Fs = 100 ms), which is commonly used in the fMRI-scanner. The raw output data was preprocessed using a custom Matlab tool (https://github.com/can-lab/brainampconverter), which applies bandpass filtering (0.3 – 3 Hz) to remove low frequency drifts. Artefacts that were time locked to the fMRI volumes were removed via deconvolution and the tool automatically detected peaks. We used another custom tool (https://github.com/can-lab/hera) for visual inspection and correction in Matlab R2020a (Mathworks Inc, Natick, MA, USA). Motion artifacts and ectopic beats, which could create sudden large changes in consecutive inter beat intervals (IBIs) (>30%), were manually removed and data were interpolated. If more than ±50% of the data was removed or had no clear visual peaks, the participant was excluded from the study. A regressor was created from the corrected HR-data. The IBIs (in seconds) were averaged in blocks of 10.5 seconds, the inverse was multiplied by 60 to get the mean bpm per data point in a block. At last, the data was demeaned, and resampled at the fMRI TR. Resampling used interpolation to the nearest neighbor in order to create a blocked regressor with the average HR values corresponding to the volume acquisition time-points.

2.5 fMRI/HR - Analysis

Structural and functional MRI data were preprocessed using fMRIPrep version 1.5.8, a modular software that combines the best preprocessing steps from other tools (Esteban et al., 2019). Preprocessed data was used for the first-level analysis and group analysis using FEAT (FMRI Expert Analysis Tool) Version 6.0 part of FSL (FMRIB's Software Library) (Jenkinson et al., 2012). In first-level analysis, image registration was turned off as this was already done in fMRIPrep, fMRI data was pre whitened and spatially smoothened (5mm FWHM) (Woolrich et al., 2001). The HR-regressors were convolved with a canonical double-gamma hemodynamic response function (HRF), a preset function that is a mixture of two Gamma functions (Friston et al., 1998). The correlation of the HR-regressor with the fMRI voxel time-series was analyzed using FILM (FMRIB's Improved Linear Model), a GLM-based model (Woolrich et al., 2001). The output showed statistical maps to MNI space, corrected for multiple comparisons using default cluster-level correction within FEAT (voxel-level $Z>3.1$, cluster-level $p<0.05$), for each participant separately (Worsley, 2001).

Group-level analysis with the individual first level outputs was carried out using FLAME (FMRIB's Local Analysis of Mixed Effects) stage 1 (Woolrich et al., 2004). Whole brain effects were analyzed with the same default cluster-level correction parameters as used in the first level analysis. Later a region of interest (ROI) analysis was done by pre-thresholding the image with a gray matter (GM) mask to ignore clusters in white matter, CSF and large arteries and increase sensitivity to GM activity. FEAT needs its own image registration matrix to run the group-level analysis, however the data was preregistered with FMRIPREP. Therefore, we made an identity matrix and let FEAT use this matrix for registration, therefore the preregistered data was not affected by FEAT with the created registration matrix. Finally, the significant clusters were evaluated for validation of the HR-data.

3. Results

3.1 Participants

Current validation-study included, after exclusion, data from 190 participants (135 females, 55 males), aged between 18 and 47 years old (mean = 22.9, std = 4.96). Age distribution is shown in **figure 1a**. Distribution of the HADS-A scores is plotted in **figure 1b**, 79% of the participants had a high HADS-A score (>7) versus 21% with scores ≤7, indicating the oversampled population (range = 0 – 16, mean = 9.0, std = 3.3). From 246 included participants, 56 participants were excluded due to a variety of reasons specified in **table 1.**

3.2 fMRI/HR analysis

Cleaning of HR-data lead to exclusion of 23 participants (**table 1**). On average 11.14 percent of the total RS time was rejected according to the rules we set (std = 11.25%, range = 0.4 – 52.4%). Blocking the HR-data to build the regressor resulted in higher rejection values as the windows have to fit between rejected periods (mean = 15.34%, std = 13.72%, range = 0.4 – 62.5%). An example HR regressor is shown in **figure 2.**

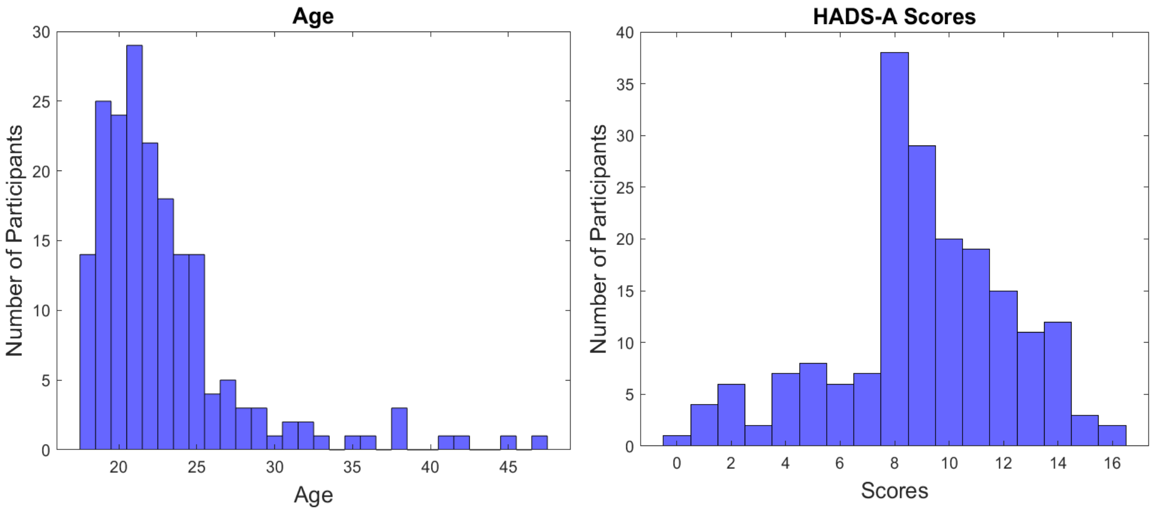

Figure 1 – Histograms from both age and HADS-A scores distribution from the included 190 participants (135 females, 55 males). Age: range = 18 – 47, mean = 22.9, std = 5.0. The distribution of the HADS-A scores (>7) shows an oversampled population with 79 percent scoring high (>7), which can be seen in the histogram as well. HADS-A: range = 0 – 16, mean = 9.0, std = 3.3.

# PARTICIPANTS	REASON FOR EXCLUSION
23	Excluded for having unusable PPG data, due to too much noise for more than ±50% of the time, or sudden IBI changes greater than 30% for more than ±50% of the time.
11	Participants showed up later, or there were problems during scanning causing delays. Because of the tight time schedule, the RS run was not done.
2	Participants did not show up or last minute cancellation. These are excluded from the large study.
2	Participants used drugs in the week before the experiment.
2	The participant did not understand a task, therefore the experiment was aborted.
1	The experiment was not done because the participant was too scared to go in the scanner.
1	Suspicion for clinical diagnosis, depression.
1	Incidental finding, highly asymmetric brain.
1	Participant had too long eyelashes for the eye tracker.
12	There was no further notice why RS data or HR-data did not exist.

Table 1 – Detailed overview of the reasons why participants were excluded from the study, and how many were excluded for that particular reason.

Results from instantaneous and blocked HR/fMRI analyses are shown in **Figure 3,** and statistically significant clusters ($p<0.05$, cluster-wise correction for multiple comparisons) at group level for positive and negative correlations between the masked imaging data and blocked HR regressor are listed in **tables 2** and **3**. In **figure 3.A** statistically significant associations were found between the instant HR and CSF or blood flowing in the ventricles or blood vessels. In total five clusters were found, one including the left and right lateral ventricle, the other four significant clusters were found outside the brain. In the analysis with the blocked regressor we found positive associations (**figure 3.B**) including bilateral PC, bilateral PCC, ACC, paracingulate gyrus (PCG), medial frontopolar lobe (mFPL) located in the ventromedial PFC (vmPFC), bilateral thalamus extending to parahippocampal gyrus (PHG), cerebellar vermis I-V, right cerebellar crus I, and a cluster in the midbrain. Negative associations (**figure 3.C**) were found in a widespread cortical cluster over the left and right hemisphere, bilateral cerebellar crus II, pons, and right thalamus.

Z-SCORE POSITIVE	MNI: X (MM)	MNI: Y (MM)	MNI: Z (MM)	HEMI-SPHERE	CLUSTER
6.97	-10	-66	28	L/R	Left and right Precuneus extending to Posterior Cingulate Cortex
7	0	-4	6	L/R	Left and Right Thalami
4.76	0	34	6	L/R	Anterior Cingulate Cortex extending to the Paracingulate Gyrus and medial Frontopolar Lobe
6.09	0	-60	-22	L/R	Cerebellar vermis I-V
4.83	52	-66	-38	R	Right Cerebellar Crus I
5.36	0	-20	-16	L/R	Midbrain
4.94	-6	-90	-22	L	-

Table 2 *– Localization of significant clusters showing positive correlation between the blocked HR-Regressor and the masked fMRI data. All coordinates are in MNI space (mm). The covered areas by the cluster are included.*

Z-SCORE NEGATIVE	MNI: X (MM)	MNI: Y (MM)	MNI: Z (MM)	HEMI-SPHERE	CLUSTER
-9.58	60	16	12	L/R	A cluster covering a large area of the cortex
-6.76	-22	-76	-42	L/R	Cerebellar left and right Crus II
-6.72	10	-30	-34	L/R	Pons
-6.45	14	-28	4	R	Right Thalamus

Table 3 *- Localization of significant clusters showing negative correlation between the blocked HR-Regressor and the masked fMRI data. All coordinates are in MNI space (mm). The covered areas by the cluster are included.*

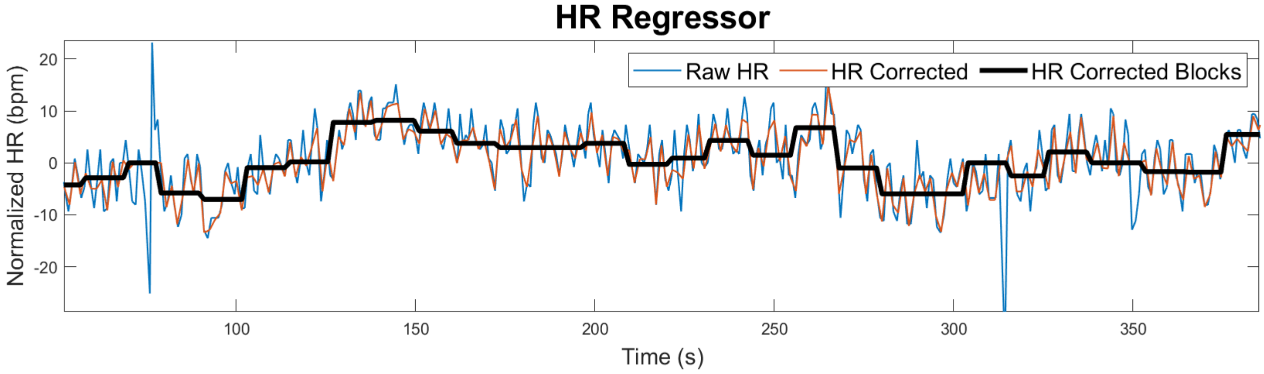

Figure 2 – Example of a normalized instantaneous windowed HR regressor in black. The blue line is raw HR-data (60/IBI) with sudden consecutive IBI changes (at 76s and 314s), which are interpolated using the Hera tool in Matlab (red line).

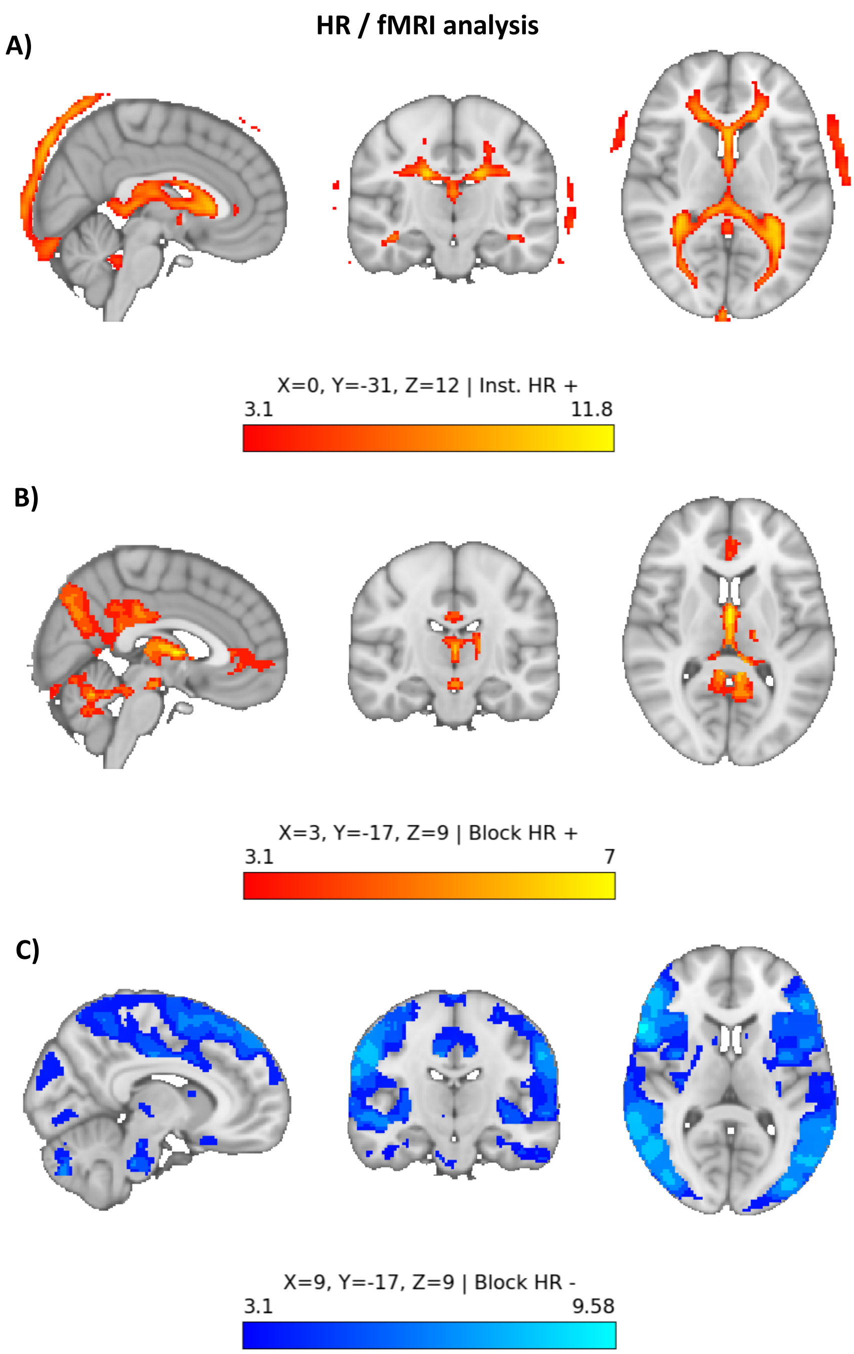

Figure 3 –Z statistic images displayed in radiological orientation showing results of the HR/fMRI analysis (Z > 3.1, color bars) and a corrected cluster significance threshold of P=0.05. The X, Y and Z coordinates shown on top of the color bars, indicate the MNI coordinates (in mm).
A) shows the positive correlation of the fMRI data with the instantaneous HR-regressor (unmasked),
B) shows the positive correlation with the blocked HR regressor including a gray matter mask applied,
C) shows the negative correlation with the blocked HR regressor including a gray matter mask applied.

4. Discussion

In this study, instantaneous and blocked continuous HR-regressors were paired with resting state fMRI-data to validate the HR-data in order to use the data for HRV analysis, and characterize the neural correlates of heart rate in a highly anxious population of ±250 participants (Brehl et al., 2021). The population was successfully oversampled for high anxiety scores as seen in **figure 1**, with 79% of the population scoring high HADS-A scores (>7), reflecting suggestive presence of an anxiety disorder (7 < score < 11) or probable presence of the mood disorder (score > 11) (Snaith, 2003). The data was collected from a larger study focusing on the neural correlates of anxiety, testing four different tasks including the RS-task (Brehl et al., 2021). In contrast with our hypothesis, we posit that the measured and preprocessed HR-data, measured with a pulse oximeter during a resting state fMRI scan, is valid and characterizes the neural correlates of cardiac activity at rest.

Group maps from instantaneous HR analysis show exclusively significant clusters outside grey and white matter regions, in the ventricles and blood vessels. In these areas, blood and cerebrospinal fluid (CSF) is moving in a pulsating flow as a result from heart contractions (Balédent et al., 2004; Farthing et al., 2007; Greitz et al., 1992). Farthing et al. (2007) found similar effects in the ventricles linked to respiration, the pressure induced respiration effects also affect the flow velocity in CSF and blood, albeit in a slower frequency than heart contractions (Farthing et al., 2007). The pulsating flow leads to a signal change that is depicted by fMRI, which leads to a decrease in sensitivity of detecting activation or false-positive activations (Farthing et al., 2007). Our findings indicate that the HR-regressor describes the pulsation effects in the brain and validates the HR-data.

Since the data was found to be valid, we were interested in the neural correlates associated with resting state cardiac control. The blocked regressor decreased artefacts from CSF and blood vessels, but they were not eliminated, therefore a GM mask was applied to the statistic images before thresholding in group-analysis (pre-thresholding). The results show significant clusters in the bilateral PCC, PC, ACC, PCG, medial FPC, right cerebellar crus I, and cerebellar vermis I-V, similar to where Valenza et al. (2019) found significant activity in their HR/fMRI analysis. Additionally, we found activity in the bilateral thalami, left PHG, while they report activity in regions of the brain other than we found in our large sample. However, they included 34 young healthy participants and differences could arise from the smaller sample size, the healthy population in comparison to our anxious population, the method of HR-data modeling, and/or the lower threshold they set for significant clusters ($Z>2.3$) (Valenza et al., 2019). We used direct HR calculations by taking the inverse of the IBI multiplied by 60, while they used point-process modelling of heartbeat dynamics (Valenza et al., 2019). The point-process model is based on the fact that effects of sympathetic and parasympathetic inputs to the SA node are not discrete in time, but persist for several seconds; quick response to vagal activity (±150 ms latency, steady state at 1-2 s) and slower sympathetic response (±1-2 s latency, steady state at 30-60 s) (Barbieri et al., 2005; Napadow et al., 2008). Point-process modelling uses a probabilistic model of heart rate dynamics in which the delayed effects of the autonomic inputs are incorporated, resulting in instantaneous HR or HRV calculations where every value is a function of the recent history of inputs (Barbieri et al., 2005). As this method accounts for the dynamic, delayed autonomic effects, it will be more sensitive to autonomic neural activity.

Another useful finding from our results is that it shows many similarities with regions involved in the default mode network (DMN) and CAN. The DMN is a resting state network that consists of a network of areas that are active during a task-free condition, including important activation in the mPFC, ACC, PCC, PC, retrosplenial cortex, inferior parietal lobe (IPL) and hippocampal areas including entorhinal cortex and PHG (Buckner et al., 2008; Nikolaou et al., 2016). The overlapping regions (mPFC, precuneus, ACC, and PHG) from our blocked HR/fMRI analysis with regions from large established networks such as the CAN and DMN indicate a stronger validation of the HR-data as both networks are involved in cardiac control. Additionally, a large negative cluster was found in the brainstem (**table 3**), in the pons, which includes regions that are found to be related to cardiovagal activity (Napadow et al., 2008). However, further analysis of areas in the brainstem that were responsible for the negative correlation is necessary as this area is more sensitive to physiological artifacts (Napadow et al., 2008). Therefore, the brainstem needs a closer look in future analyses. In the study of Napadow et al. (2008) they did focus on the brainstem in autonomic influences of HF-HRV. In order to reduce physiological artefacts, they measured HR via electrocardiography (ECG) and cardiac-gated the fMRI acquisition by synchronizing the start of a new acquisition with the occurrence of the R-top in ECG. Hence, all acquisitions are made at the same time in a cardiac cycle which limits the cardiovascular artefacts by vessels in and around the brain, but there are different TRs (Napadow et al., 2008). This seems to be a useful method for reducing vascular artefacts by cardiac activity, when correcting for the different T1-effects which influence the signal, caused by the variable TRs.

Comparing our findings with studies that focused on neural autonomic modulation of the heart, we could distinguish brain regions that are directly influenced by HR fluctuations, and that are involved in parasympathetic HR control. The insula and amygdala are regularly found to be involved in autonomic modulation, but we did not find a correlation between these regions and low frequency HR fluctuations in our experiment (Critchley et al., 2003; Thayer et al., 2012; Valenza et al., 2017). This could mean that the insula has no direct relation to HR fluctuations, but is active in central autonomic modulation as a relay center. A meta-analysis including eight neuroimaging studies, in total 191 participants, showed significant activations in relation to HRV in the vmPFC (Thayer et al., 2012). They conclude that this region is integrated with brainstem regions which directly regulate the heart rate. This goes along with our findings of activity in anterior cingulate and frontopolar regions. The relation between prefrontal regions and heart rate control may partly explain decreased heart rate control and lower HRV in patients with anxiety disorders showing aberrant activity in prefrontal regions (Brehl et al., 2020; Thayer et al., 2012).

Remarkably, we found widespread negative correlations with HR fluctuations in GM, which contains large draining veins and is highly vascularized (Shmueli et al., 2007). The observed BOLD fMRI signal in ventricles and blood vessels depends on oxygenation, blood flow and volume (Shmueli et al., 2007). According to the Monro-Kellie doctrine, modified by Weed, the intracranial volume including arterial blood, venous blood, capillary blood, and CSF remains constant during a cardiac cycle (Kellie, 1824; Monro, 1783; Weed, 1929). Heart contractions cause the intracranial arteries to fill with blood and expand. The increase in arterial volume is counteracted by CSF flowing from the ventricles into the spinal cord, causing an increased BOLD signal from CSF in the ventricles by the increased flow, synchronized with the arterial filling after the heart beat (Greitz et al., 1992). This could explain the positive correlation in the ventricles and arteries around the brain as seen in **Figure 3.A**. Another effect from arterial volume increase, is a slight counteracting decrease in venous volume and pulsations, potentially explaining the negative correlation in the highly vascularized GM containing large draining veins (**Figure 3.C**) (Greitz et al., 1992). **Figure 4** shows a diagram indicating the relationship between the different volumes. Shmueli et al. found similar widespread negative cortical correlations for LF heartbeat variations, with the strongest negative correlations at time shifts of 6-12 seconds (Shmueli et al., 2007). Because of high vascularization of GM, it has greater BOLD signal and fluctuations, which could explain why very weak correlations with the HR regressor seem stronger in the GM (Shmueli et al., 2007). Therefore, the negative clusters has to be considered with caution, as these activations could be artefacts.

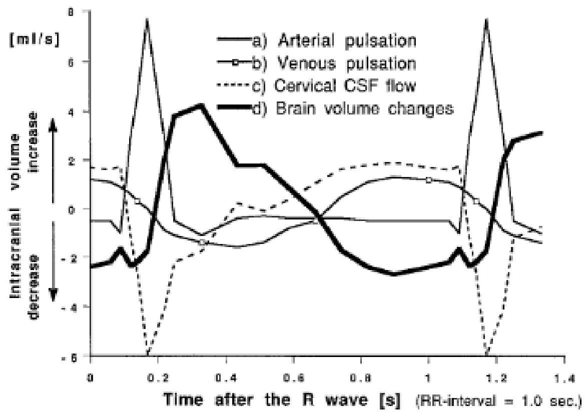

Figure 4 – Diagram showing the interaction between intracranial volume changes. Arterial pulsation, venous pulsation and CSF flow measurements were taken from recordings at the foramen magnum. The sum of these three measurements is displayed as the total brain volume changes. Image adapted from: (Greitz et al., 1992)

Measuring HR via PPG-waveforms is a non-invasive and easy method by applying a pulse oximeter clip at a peripherally vascularized region such as the earlobe or finger, but it is sensitive to scanner and motion artefacts or distortions due to bad contact. In our experiment, a pulse oximeter was placed at the index finger. The obtained data is filtered to remove unwanted signal such as drift and artefacts that arise from radiofrequency pulses by the fMRI scanner. The filter could create filter artefacts which could contaminate the data. However, literature showed that PPG proves to be a reliable measure compared to the more invasive, but more precise ECG for measuring HR and HRV (Selvaraj et al., 2008). As explained in the introduction, PVCs and artefacts need to be detected and removed from the data. Motion artefacts that are not removed by filtering are easily detectable by sudden large transients in the data, however PVCs are harder to recognize. PVCs are usually benign and result in two consecutive beats with a short inter beat interval (IBI), followed by a compensatory delay (Kamath et al., 2013). It is not clear when the total effects of an ectopic beat are ceased, because ectopic beats lead to transient drops in blood pressure that activates autonomic responses that could last for 10-30 beats (Kamath et al., 2013). To correct for potential PVCs, we chose to remove consecutive IBIs which had more than 30% difference in time (Kemper et al., 2007). However, some papers advise to be more strict and set the threshold at 20% changes between consecutive IBIs (Kamath et al., 2013; Malik et al., 1996). The rejected period was interpolated, and in order to not create false variability or remove too much data; the start and end of the rejected period should have similar IBIs. Similar rules were used for removal of motion artefacts, or regions with bad data quality due to less effective contact. PVCs in healthy persons can have multiple triggers such as caffeine, alcohol, drugs, exercise, sleep apnea, stress, and anxiety (Frigy et al., 2018). In data from several participants, we found many (>10) IBI differences exceeding the 30% threshold, which could indicate PVCs triggered by anxiety in our anxious population.

Consequently, by removing PVCs and focusing on heartbeats that arise from the SA-node, the effect of the heart on the brain is decreased. Notwithstanding, PVCs can influence brain activity as they influence blood pressure, which leads to different feedback from baroreceptors to the ANS. Additionally, the intrinsic cardiac nervous system (ICNS), which is called the little brain of the heart, influences the heart function by modulating the contractility, relaxation, heart rate, conduction velocity, and myocyte adhesion (Fedele and Brand, 2020). Hence, correlating HR with fMRI would not only reflect areas that control HR, but also areas that are influenced by the heart. For studying the influence of a task on autonomic control of the heart, it is advisable to consider these reciprocal feedback mechanisms.

Correlating simultaneously measured blocked HR data with fMRI data during RS proved to be a useful method to validate peripheral HR-data and find neural correlates involved in cardiac control. Our data could be validated and can be used for further analyses with calculations of HRV. The tool we used for correcting HR-data automatically calculates the root mean square of the standard deviations between consecutive IBIs (RMSSD), which is a measure for HRV (Catai et al., 2020; Kamath et al., 2013; Shaffer and Ginsberg, 2017). When focusing at parasympathetic vagal modulations of the heart, the high frequency content is a good parameter for modeling the PNS activity (Thayer et al., 2012). However, point-process modeling might be the superior method by focusing more on the biological processes that arise from vagal modulation, and should be considered for calculating instantaneous heartbeat dynamics (Barbieri et al., 2005). Our findings showed neural correlates that are directly involved with HR fluctuations by either regulation of the HR or processing the feedback from the heart. Future research with this large dataset using HF and LF HRV could increase focus on the neural correlates of autonomic modulation of the heart.

5. References

Balédent, O., Gondry-Jouet, C., Meyer, M.E., De Marco, G., Le Gars, D., Henry-Feugeas, M.C., Idy-Peretti, I., 2004. Relationship between Cerebrospinal Fluid and Blood Dynamics in Healthy Volunteers and Patients with Communicating Hydrocephalus. Invest. Radiol. 39, 45–55. https://doi.org/10.1097/01.rli.0000100892.87214.49

Barbieri, R., Matten, E.C., Alabi, A.R.A., Brown, E.N., 2005. A point-process model of human heartbeat intervals: New definitions of heart rate and heart rate variability. Am. J. Physiol. - Hear. Circ. Physiol. 288, 424–435. https://doi.org/10.1152/ajpheart.00482.2003

Benarroch, E.E., 2012. Central Autonomic Control. Prim. Auton. Nerv. Syst. 9–12. https://doi.org/10.1016/B978-0-12-386525-0.00002-0

Benarroch, E.E., 1993. The Central Autonomic Network: Functional Organization, Dysfunction, and Perspective. Mayo Clin. Proc. 68, 988–1001. https://doi.org/10.1016/S0025-6196(12)62272-1

Brehl, A.K., Kohn, N., Schene, A.H., Fernández, G., 2021. Neural diversity in the anxious phenotype: An fMRI-based clustering approach to capture individual differences in pathology-related neural activation profiles (Unpublished doctoral dissertation). Donders Inst. Brain Cogn. Behav. Dep. Cogn. Neurosci. Psychiatry, Radboud Univ. Med. Center, Nijmegen, Netherlands.

Brehl, A.K., Kohn, N., Schene, A.H., Fernández, G., 2020. A mechanistic model for individualised treatment of anxiety disorders based on predictive neural biomarkers. Psychol. Med. https://doi.org/10.1017/S0033291720000410

Buckner, R.L., Andrews-Hanna, J.R., Schacter, D.L., 2008. The brain's default network: Anatomy, function, and relevance to disease. Ann. N. Y. Acad. Sci. 1124, 1–38. https://doi.org/10.1196/annals.1440.011

Catai, A.M., Pastre, C.M., Godoy, M.F. de, Silva, E. da, Takahashi, A.C. de M., Vanderlei, L.C.M., 2020. Heart rate variability: are you using it properly? Standardisation checklist of procedures. Brazilian J. Phys. Ther. 24, 91–102. https://doi.org/10.1016/j.bjpt.2019.02.006

Chalmers, J.A., Quintana, D.S., Abbott, M.J.A., Kemp, A.H., 2014. Anxiety disorders are associated with reduced heart rate variability: A meta-analysis. Front. Psychiatry 5, 1–11. https://doi.org/10.3389/fpsyt.2014.00080

Critchley, H.D., Mathias, C.J., Josephs, O., O'Doherty, J., Zanini, S., Dewar, B.K., Cipolotti, L., Shallice, T., Dolan, R.J., 2003. Human cingulate cortex and autonomic control: Converging neuroimaging and clinical evidence. Brain 126, 2139–2152. https://doi.org/10.1093/brain/awg216

Esteban, O., Markiewicz, C.J., Blair, R.W., Moodie, C.A., Isik, A.I., Erramuzpe, A., Kent, J.D., Goncalves, M., DuPre, E., Snyder, M., Oya, H., Ghosh, S.S., Wright, J., Durnez, J., Poldrack, R.A., Gorgolewski, K.J., 2019. fMRIPrep: a robust preprocessing pipeline for functional MRI. Nat. Methods 16, 111–116. https://doi.org/10.1038/s41592-018-0235-4

Farthing, J.P., Cummine, J., Borowsky, R., Chilibeck, P.D., Binsted, G., Sarty, G.E., 2007. False activation in the brain ventricles related to task-correlated breathing in fMRI speech and motor paradigms. Magn. Reson. Mater. Physics, Biol. Med. 20, 157–168. https://doi.org/10.1007/s10334-007-0077-z

Fedele, L., Brand, T., 2020. The intrinsic cardiac nervous system and its role in cardiac pacemaking and conduction, Journal of Cardiovascular Development and Disease. https://doi.org/10.3390/jcdd7040054

Frigy, A., Csiki, E., Caraşca, C., Szabó, I.A., Moga, V.D., 2018. Autonomic influences related to frequent ventricular premature beats in patients without structural heart disease. Med. (United States) 97. https://doi.org/10.1097/MD.0000000000011489

Friston, K.J., Fletcher, P., Josephs, O., Holmes, A., Rugg, M.D., Turner, R., 1998. Event-related fMRI: Characterizing differential responses. Neuroimage 7, 30–40. https://doi.org/10.1006/nimg.1997.0306

Greitz, D., Wirestam, R., Franck, A., Nordell, B., Thomsen, C., Stfihlberg, F., 1992. Diagnostic Neuroradiology Pulsatile brain movement and associated hydrodynamics studied by magnetic resonance phase imaging The Monro-Kellie doctrine revisited, Neuroradiology.

Jenkinson, M., Beckmann, C.F., Behrens, T.E.J., Woolrich, M.W., Smith, S.M., 2012. FSL. Neuroimage 62, 782–790. https://doi.org/https://doi.org/10.1016/j.neuroimage.2011.09.015

Kamath, M. V., Watanabe, M.A., Upton, A.R.M., 2013. Heart rate variability (HRV) signal analysis: Clinical applications, Heart Rate Variability (HRV) Signal Analysis: Clinical Applications.

Kellie, G., 1824. An Account of the Appearances Observed in the Dissection of Two of Three Individuals Presumed to Have Perished in the Storm of the 3d, and Whose Bodies Were Discovered in the Vicinity of Leith on the Morning of the 4th, November 1821; with Some Reflection. Trans. Medico-Chirurgical Soc. Edinburgh 1, 84–122.

Kemper, K.J., Hamilton, C., Atkinson, M., 2007. Heart rate variability: Impact of differences in outlier identification and management strategies on common measures in three clinical populations. Pediatr. Res. 62, 337–342. https://doi.org/10.1203/PDR.0b013e318123fbcc

Kim, Y.K., Yoon, H.K., 2018. Common and distinct brain networks underlying panic and social anxiety disorders. Prog. Neuro-Psychopharmacology Biol. Psychiatry 80, 115–122. https://doi.org/10.1016/j.pnpbp.2017.06.017

Lacey, J.I., 1967. Somatic response patterning and stress: Some revisions of activation theory, in: Psychological Stress. pp. 246–285.

Lane, R.D., McRae, K., Reiman, E.M., Chen, K., Ahern, G.L., Thayer, J.F., 2009. Neural correlates of heart rate variability during emotion. Neuroimage 44, 213–222. https://doi.org/10.1016/j.neuroimage.2008.07.056

Malik, M., John Camm, A., Thomas Bigger, J., Breithardt, G., Cerutti, S., Cohen, R.J., Coumel, P., Fallen, E.L., Kennedy, H.L., Kleiger, R.E., Lombardi, F., Malliani, A., Moss, A.J., Rottman, J.N., Schmidt, G., Schwartz, P.J., Singer, D.H., 1996. Heart rate variability: Standards of measurement, physiological interpretation, and clinical use. Circulation 93, 1043–1065. https://doi.org/10.1161/01.cir.93.5.1043

Monro, A., 1783. Observations on the structure and functions of the nervous system. Edinburgh 4, 113–135.

Napadow, V., Dhond, R., Conti, G., Makris, N., Brown, E.N., Barbieri, R., 2008. Brain correlates of autonomic modulation: Combining heart rate variability with fMRI. Neuroimage 42, 169–177. https://doi.org/10.1016/j.neuroimage.2008.04.238

Nikolaou, F., Orphanidou, C., Papakyriakou, P., Murphy, K., Wise, R.G., Mitsis, G.D., 2016. Spontaneous physiological variability modulates dynamic functional connectivity in resting-state functional magnetic resonance imaging. Philos. Trans. R. Soc. A Math. Phys. Eng. Sci. 374. https://doi.org/10.1098/rsta.2015.0183

Selvaraj, N., Jaryal, A., Santhosh, J., Deepak, K.K., Anand, S., 2008. Assessment of heart rate variability derived from finger-tip photoplethysmography as compared to electrocardiography. J. Med. Eng. Technol. 32, 479–484. https://doi.org/10.1080/03091900701781317

Shaffer, F., Ginsberg, J.P., 2017. An Overview of Heart Rate Variability Metrics and Norms. Front. Public Heal. 5, 1–17. https://doi.org/10.3389/fpubh.2017.00258

Shaffer, F., McCraty, R., Zerr, C.L., 2014. A healthy heart is not a metronome: an integrative review of the heart's anatomy and heart rate variability. Front. Psychol. 5, 1–19. https://doi.org/10.3389/fpsyg.2014.01040

Shmueli, K., van Gelderen, P., de Zwart, J.A., Horovitz, S.G., Fukunaga, M., Jansma, J.M., Duyn, J.H., 2007. Low-frequency fluctuations in the cardiac rate as a source of variance in the resting-state fMRI BOLD signal. Neuroimage 38, 306–320. https://doi.org/https://doi.org/10.1016/j.neuroimage.2007.07.037

Sklerov, M., Dayan, E., Browner, N., 2019. Functional neuroimaging of the central autonomic network: recent developments and clinical implications. Clin. Auton. Res. 29, 555–566. https://doi.org/10.1007/s10286-018-0577-0

Smith, T.W., Houston, B.K., Stucky, R.J., 1985. Effects of threat of shock and control over shock on finger pulse volume, pulse rate and systolic blood pressure. Biol. Psychol. 20, 31–38. https://doi.org/10.1016/0301-0511(85)90039-0

Snaith, R.P., 2003. The hospital anxiety and depression scale. Health Qual. Life Outcomes 1, 6–9. https://doi.org/10.1186/1477-7525-1-29

Sološenko, A., Petrenas, A., Marozas, V., 2015. Photoplethysmography-Based Method for Automatic Detection of Premature Ventricular Contractions. IEEE Trans. Biomed. Circuits Syst. 9, 662–669. https://doi.org/10.1109/TBCAS.2015.2477437

Thayer, J.F., Åhs, F., Fredrikson, M., Sollers, J.J., Wager, T.D., 2012. A meta-analysis of heart rate variability and neuroimaging studies: Implications for heart rate variability as a marker of stress and health. Neurosci. Biobehav. Rev. 36, 747–756. https://doi.org/10.1016/j.neubiorev.2011.11.009

Valenza, G., Duggento, A., Passamonti, L., Diciotti, S., Tessa, C., Barbieri, R., Toschi, N., 2017. Resting-state brain correlates of instantaneous autonomic outflow. Proc. Annu. Int. Conf. IEEE Eng. Med. Biol. Soc. EMBS 3325–3328. https://doi.org/10.1109/EMBC.2017.8037568

Valenza, G., Sclocco, R., Duggento, A., Passamonti, L., Napadow, V., Barbieri, R., Toschi, N., 2019. The central autonomic network at rest: Uncovering functional MRI correlates of time-varying autonomic outflow. Neuroimage 197, 383–390. https://doi.org/10.1016/j.neuroimage.2019.04.075

Weed, L.H., 1929. Some Limitations of the Monro-Kellie Hypothesis, in: Archives of Surgery. p. 1049. https://doi.org/10.1001/archsurg.1929.01140130137006

Woolrich, M.W., Behrens, T.E.J., Beckmann, C.F., Jenkinson, M., Smith, S.M., 2004. Multilevel linear modelling for FMRI group analysis using Bayesian inference. Neuroimage 21, 1732–1747. https://doi.org/10.1016/j.neuroimage.2003.12.023

Woolrich, M.W., Ripley, B.D., Brady, M., Smith, S.M., 2001. Temporal autocorrelation in univariate linear modeling of FMRI data. Neuroimage 14, 1370–1386. https://doi.org/10.1006/nimg.2001.0931

Worsley, K.J., 2001. Statistical analysis of activation images, in: Functional Magnetic Resonance Imaging. Oxford University Press, Oxford. https://doi.org/10.1093/acprof:oso/9780192630711.003.0014